

Micro- and nanoscale non-ideal gas Poiseuille flows in a consistent Boltzmann algorithm model

Moran Wang and Zhixin Li

Department of Engineering Mechanics, Tsinghua University, Beijing 100084, People's Republic of China

Received 9 January 2004, in final form 19 March 2004

Published 4 June 2004

Online at stacks.iop.org/JMM/14/1057

doi:10.1088/0960-1317/14/7/028

Abstract

The direct simulation Monte Carlo method in the consistent Boltzmann algorithm model has been developed and expanded for non-ideal gas predictions. The enhanced collision rate factor is determined by considering the excluded molecular volume and shadowing/screening effects based on the Enskog theory. The parameter for the attraction strength is also determined by comparison with the classical thermodynamics theory. Different pressure-driven gas Poiseuille flows in micro- and nanoscale channels are investigated. The van der Waals effect leads to a higher mass flow rate and different friction and heat transfer characteristics on the wall surface, compared to the results in the perfect gas model. The results also show that the van der Waals effect is dependent not only on the pressure but also on the channel size. A higher driving pressure or a smaller channel size will result in a larger van der Waals gas effect.

1. Introduction

For high-Knudsen-number fluid, the continuum-based equations fail to give qualitatively correct predictions on flow behavior and heat transfer characteristics [1, 2]. The fluid must be described from a molecular point of view and the Boltzmann equation is the governing equation [3]. However, unfortunately, the Boltzmann equation can hardly be solved analytically or numerically due to its complicated nonlinear collision integral term, except in some special cases [4]. The direct simulation Monte Carlo method (DSMC) according to Bird [5] is one successful method based on statistics-mechanics to simulate rarefied gases [6], and it has been rigorously proved equivalent to a numerical solution of the Boltzmann equation for rarefied gas flows [7]. For the gas flows in micro or nano systems, the Knudsen number can also be quite high due to a small characteristic length though the gas may indeed be dense. Several researchers have applied DSMC for simulations of gas flows in micro and nano channels [8–12].

In most of the previous simulations, the variable hard sphere (VHS) model was used. In this model, the attractive potential was ignored and the gas was treated as a perfect gas so that a high-density-small-scale flow can be treated to be similar

to a low-density-large-scale flow as long as the Knudsen and Mach numbers and the boundary conditions are the same [2, 13]. Hassan and Hash [14] developed a generalized hard sphere (GHS) model and Fan [15] developed a generalized soft sphere (GSS) model, by considering the attractive potential of molecular interactions. However, the attractive potential only depended on temperature in the two models. It is known that when the gas is quite dense, the van der Waals force will become important, and the van der Waals equation will replace the Clapeyron equation to be the equation of state (EOS). It is then noted that both DSMC and the Boltzmann equation are inconsistent since the collision rate and transport properties are functions of the particles' cross-section while the EOS is not. This may be the reason why the DSMC cannot simulate the dense effect of gas flow, where the van der Waals force is important [16].

Several researchers have done foundational work for dense gas simulations [16–19]. A consistent Boltzmann algorithm (CBA) proposed by Alexander *et al* [16] modified the DSMC method according to the van der Waals equation and expanded DSMC to dense gas even liquid. The nuclear flow [20] and the surface properties of a van der Waals fluid [21] have been simulated using DSMC in the CBA model. In

the present paper, the CBA model is developed for the nitrogen gas. The enhanced collision rate is determined by considering the excluded molecular volume and shadowing/screening effects based on the Enskog theory. The parameter for the attraction strength is also determined by a comparison with the classical thermodynamics theory. The pressure-driven plane Poiseuille flows are then simulated for different domain sizes and different pressure boundaries using the CBA model. The results are compared with those from the perfect gas model. Finally, the van der Waals effect dependences on the gas density and on the flow characteristic length are discussed.

2. Numerical method

2.1. DSMC method

DSMC is a molecular-based statistical simulation method for rarefied gas flow introduced by Bird [5]. The method numerically solves the dynamic equations for gas flow using thousands of simulated molecules. Each simulated molecule represents a large number of real molecules. With the assumption of molecular chaos and a rarefied gas, only the binary collisions are considered, so the molecular motion and their collisions are uncoupled if the computational time step is smaller than the physical collision time. The interactions with boundaries and with other molecules conserve both momentum and energy. The macroscopic flow characteristics are obtained statistically by sampling the molecular properties in each cell. At the beginning of the calculation, the simulated particles are uniformly distributed statistically in the cells. At each time step, all particles move according to their individual velocities, interact with the boundaries and are then indexed. In each cell, a certain number of collision pairs are selected using the no-time-counter (NTC) method and collisions are calculated. These steps are repeated until the statistical errors are small enough.

2.2. CBA model

The CBA model was first introduced in 1995 [16]. It extends the DSMC method to a van der Waals fluid. In the CBA model, a weak and constant potential to the hard core is considered according to the van der Waals EOS. The method for the CBA modification in the advection process to obtain the van der Waals EOS is described below.

For a hard-sphere gas, the CBA introduces a correlation by displacing the particles in the advection step of $\mathbf{d}_{\text{HS}} = \sigma \hat{\mathbf{d}}$, where σ is the particle diameter and the unit vector $\hat{\mathbf{d}}$ is

$$\hat{\mathbf{d}} = \frac{(v'_i - v'_j) - (v_i - v_j)}{|(v'_i - v'_j) - (v_i - v_j)|} = \frac{\mathbf{v}'_r - \mathbf{v}_r}{|\mathbf{v}'_r - \mathbf{v}_r|}, \quad (1)$$

where \mathbf{v}_r is the relative velocity of the colliding particles. The primed and unprimed velocities indicate post- and precollision values, respectively. After the collision, the particles are advected as

$$\mathbf{r}_i(t + \Delta t) = \mathbf{r}_i(t) + \mathbf{v}'_i(t)\Delta t + \mathbf{d}_{\text{HS}}, \quad (2)$$

$$\mathbf{r}_j(t + \Delta t) = \mathbf{r}_j(t) + \mathbf{v}'_j(t)\Delta t - \mathbf{d}_{\text{HS}}. \quad (3)$$

Equation (1) leads to an average virial $\Theta = \sigma \sqrt{\pi kT/m}$, where m is the molecular mass. By using the Boltzmann

collision rate for dilute gas, $\Gamma_B = 2\sigma^2 n^2 \sqrt{\pi kT/m}$, the consistent pressure is now $P = nkT(1 + b_2 n)$, where $b_2 = \frac{2}{3}\pi\sigma^3$ is the second virial coefficient and n is the molecular number density. By introducing the Enskog Y factor into the CBA, which corrects the low-density collision rate to the correct hard-sphere collision rate at any density [$\Gamma_{\text{HS}} = Y(n)\Gamma_B$], the correct EOS at all densities and transport coefficients at high-densities are obtained corresponding to an uncorrelated collision (Markov) approximation.

By changing the advection displacement to account for the attractive force, the CBA is generalized to yield the van der Waals EOS, which is

$$\frac{P_{\text{vdW}}}{nkT} = 1 + b_2 n Y - \frac{a n}{kT}, \quad (4)$$

where a represents the attraction strength and the magnitude of the displacement is [23]

$$d_{\text{vdW}} = \sigma - \frac{a\sigma}{b_2 Y kT} = d_{\text{HS}} - d_a. \quad (5)$$

The gas transport properties were changed by introducing the displacement d_{vdW} , and a random displacement was tried to adjust the transport properties independent of the EOS [22–24]. However, in the cases studied in the present paper, the gas transport coefficients remain close to the actual values for hard spheres.

2.3. Parameter determination

The CBA model expands the DSMC method to van der Waals fluids in theory, and has been used for analyzing dense fluid behaviors, such as nuclear flows [20] and gas–liquid surface properties [21]. However, the previous investigations were limited to qualitative analysis due to undetermined attraction strength. The Y factors of the enhanced collision rate were quite different for different researchers [17–24]. Here the Y factor is determined strictly on the basis of the Enskog theory for dense gases, and the attraction strength is obtained by comparing with the classical thermodynamics theory.

Based on the Enskog equation for dense gas [25] when a gas is so dense that the covolume of the molecules is comparable with the total volume of the system, the molecules can no longer be treated as point particles. Therefore, the common position of two colliding molecules in the Boltzmann equation should be replaced by the actual positions of the centers of two tangent spheres, and the collision frequency is influenced by correlational effects that depend on the density at the point of contact. Due to the reduced volume occupied by molecules, a modified higher scattering probability is

$$\Gamma' = \frac{V}{V'} \Gamma_B, \quad (6)$$

where $V' = (1 - n \frac{4}{3}\pi\sigma^3)$. However, the scattering probability is lowered again by another effect, namely that the particles are screening each other. A particle might not be available for scattering with another particle because there might be a third particle in between. This effect leads to a reduction of the scattering probability by a factor of $(1 - n \frac{11}{12}\pi\sigma^3)$. Including this factor, the modified scattering probability is

$$\Gamma_{\text{HS}} = Y(n)\Gamma_B, \quad (7)$$

where $Y(n) = \frac{1 - 11nb_2/8}{1 - 2nb_2}$.

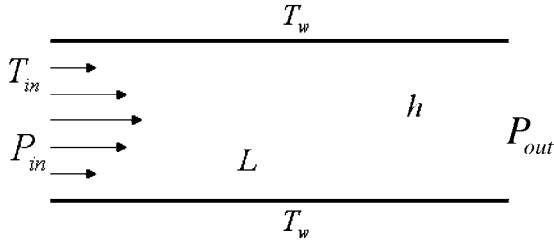


Figure 1. Schematic of the physical problem.

This result can, however, be trusted only to the early orders in n , since four particle configurations have not been considered [25]. In the current study, the expression up to third order is used

$$Y(n) = 1 + 0.625nb_2 + 0.2869(nb_2)^2 + 0.1103(nb_2)^3. \quad (8)$$

The attractive strength is difficult to determine based on the molecular theory. Here, we compared equation (4) with the van der Waals equation from the classical thermodynamics [26], and obtained,

$$a = \frac{27 R^2 T_c^2}{64 P_c} m^2, \quad (9)$$

where R denotes the gas constant, T_c is the critical temperature and P_c is the critical pressure.

2.4. Results and discussion

The standard DSMC code of Bird [5] was developed on the basis of the CBA and the Enskog theory for dense gases. Bird's standard NTC was enhanced by a Y factor to embody the finite density effects. An additional displacement was introduced for the intermolecular attraction. The two-dimensional plane Poiseuille flows were then simulated. The basic channel configuration is shown in figure 1. The channel is L in length and h in height. The inlet pressure P_{in} , the inlet temperature T_{in} and the outlet pressure P_{out} are given.

Fifteen cases for nitrogen gas flows were considered in this paper, which were listed in table 1. The outlet pressure P_{out} was fixed at unity standard atmosphere pressure. The inlet pressure P_{in} ranged from 1.5 to 45×10^5 Pa. Both the wall temperature and the entering gas temperature were 300 K. The aspect ratio L/H was set at 5 for all simulated cases, and the channel length ranged from 0.05 to 5 μm . The Knudsen numbers are calculated on the basis of the ideal gas assumption. The 100×60 uniform rectangular cells with 4×4 subcells were used. According to Alexander *et al* [27] and Bird [5], it is required that the subcell size must be smaller than the local gas mean free path, otherwise, the gas transport coefficients will depart from the real values with changing cell size. Table 1 lists the subcell width to mean free path ratio at the inlet, where the mean free path is calculated on the basis of the ideal gas model. For cases 4 and 5, the requirement is not fulfilled near the inlet; however, the effects are limited due to the quick pressure drop along the channel. The time step for each case was half of the mean collision time at the inlet [28].

The properties of the nitrogen gas are listed in table 2, see Bird [5] and Aston and Fritz [25]. For this diatomic gas, the Larsen–Borgnakke model with discrete rotational energy is used to model the energy exchange between the translational and internal modes. The vibrational energy is assumed to be negligible. On the wall surface, the diffuse reflection model is applied, which is commonly used in micro gas simulations at present. Liou's implicit pressure boundary conditions are used [29]. For each case, the final total number of molecules is around 10^5 , and the sample size is larger than 5×10^5 . Convergence was also verified by monitoring mass balance; maximum errors were approximately 1%.

Based on the statistical and dynamical theories, the macroscopic physical quantities are obtained as follows:

$$u_j = \frac{1}{N_j} \sum u, \quad (10)$$

where u is the velocity component of each molecule, N_j is the molecule number in the cell j and u_j is the averaged

Table 1. Conditions and parameters of studied cases.

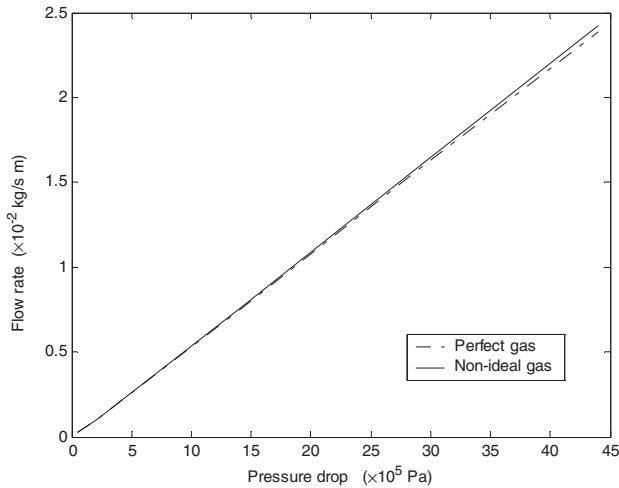
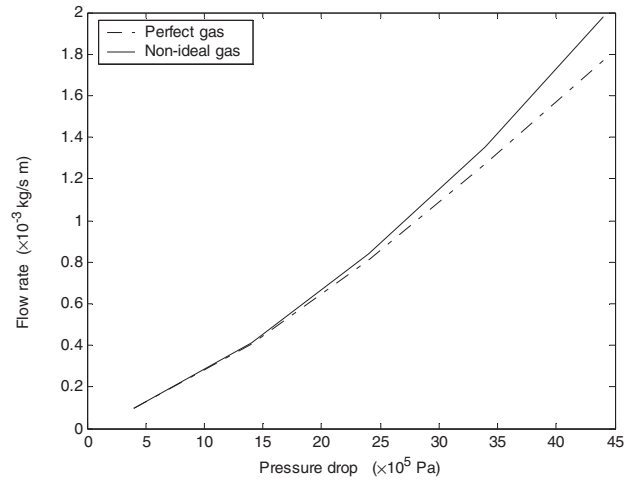
Cases	L (μm)	h (μm)	P_{in} ($\times 10^5$ Pa)	Kn_{in}	Kn_{out}	$L_{y,\text{subcell}}/\lambda_{in,\text{ideal}}$
1	5	1	1.5	0.0357	0.0536	0.10
2	5	1	3.0	0.0179	0.0536	0.20
3	5	1	15	0.00357	0.0536	1.02
4	5	1	30	0.00179	0.0536	2.05
5	5	1	45	0.00119	0.0536	3.07
6	0.5	0.1	5	0.107	0.536	0.03
7	0.5	0.1	15	0.0357	0.536	0.10
8	0.5	0.1	25	0.0214	0.536	0.17
9	0.5	0.1	35	0.0153	0.536	0.24
10	0.5	0.1	45	0.0119	0.536	0.31
11	0.05	0.01	5	1.07	5.361	0.003
12	0.05	0.01	15	0.357	5.361	0.010
13	0.05	0.01	25	0.214	5.361	0.017
14	0.05	0.01	35	0.153	5.361	0.024
15	0.05	0.01	45	0.119	5.361	0.031

L is the channel length; h is the channel height; P_{in} is the inlet pressure; Kn_{in} is the Knudsen number at inlet; Kn_{out} is the Knudsen number at outlet; $L_{y,\text{subcell}}$ is the subcell width and $\lambda_{in,\text{ideal}}$ is the mean free path at the inlet calculated on the basis of ideal equation of state.

Table 2. Properties of nitrogen gas.

m (kg)	ζ	d_{ref} (m)	T_{ref} (K)	ω	γ	T_c (K)	P_c (Pa)
4.65×10^{-26}	2	4.17×10^{-10}	273	0.74	1.4	126.2	3.39×10^6

m is the gas molecular mass, ζ is the internal energy degrees of freedom, d_{ref} is the reference molecular diameter, T_{ref} is the reference temperature, ω is the viscosity-temperature index and γ is the specific heat ratio.


Figure 2. Mass flow rate versus pressure drop for a $5 \mu\text{m} \times 1 \mu\text{m}$ channel.

Figure 3. Mass flow rate versus pressure drop for a $0.5 \mu\text{m} \times 0.1 \mu\text{m}$ channel.

x -directional velocity component for the cell j .

$$\rho_j = n_j m, \quad (11)$$

where n_j is the number density for cell j .

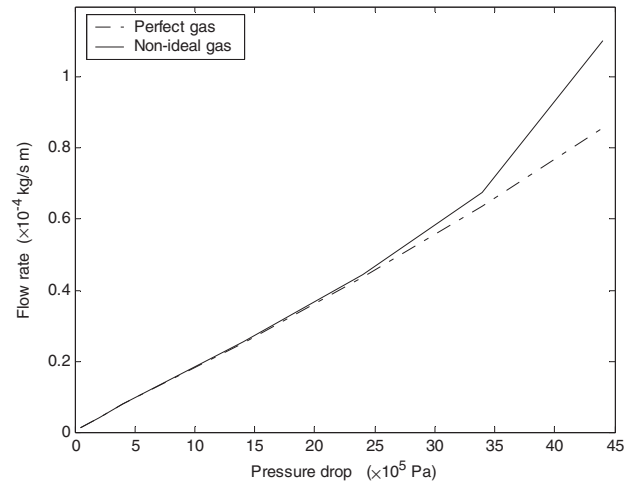
The mass flow rate is

$$Q = \int_A \rho u \, dA, \quad (12)$$

where A is a cross section area of the channel. For a 2D x -directional channel flow, equation (12) is simplified as

$$Q = \sum \rho_j u_j \Delta y_j. \quad (13)$$

The mass flow rates versus driven pressure drops at different channel scales are shown in figures 2–4, compared with the perfect gas results under the same boundaries. Figure 2 shows the results for a channel having a size of $5 \mu\text{m} \times 1 \mu\text{m}$ under different pressure boundary conditions, including cases 1–5 listed in table 1. It is shown from the comparison between perfect gas and non-ideal gas that the van der Waals effect is very small for such a micro channel even under a high driving pressure. The flow rate for non-ideal gas separates clearly from that for perfect gas at over 30×10^5 Pa driving pressure, and the maximum departure between both is less than 1.51%. The results for a $0.5 \mu\text{m} \times 0.1 \mu\text{m}$ channel (cases 6–10) are shown in figure 3. In these cases, the channel size is smaller, however, the results show that the van der Waals effect becomes more significant. The non-ideal gas flow rate separates from the perfect gas at about 25×10^5 Pa pressure. The mass flow rate in the non-ideal gas model


Figure 4. Mass flow rate versus pressure drop for a $0.05 \mu\text{m} \times 0.01 \mu\text{m}$ channel.

is 12.09% higher than that in the perfect gas model for the 44×10^5 Pa driving pressure drop. Figure 4 shows the results for a channel having a size of $0.05 \mu\text{m} \times 0.01 \mu\text{m}$ (cases 10–15). The van der Waals effect appears at about 25×10^5 Pa driving pressure. The maximum departure reaches 28.63% for the 44×10^5 Pa driving pressure drop.

It is indicated from figures 2–4 that the effect of van der Waals force on the mass flow rate of Poiseuille flow enlarges as the channel size decreases.

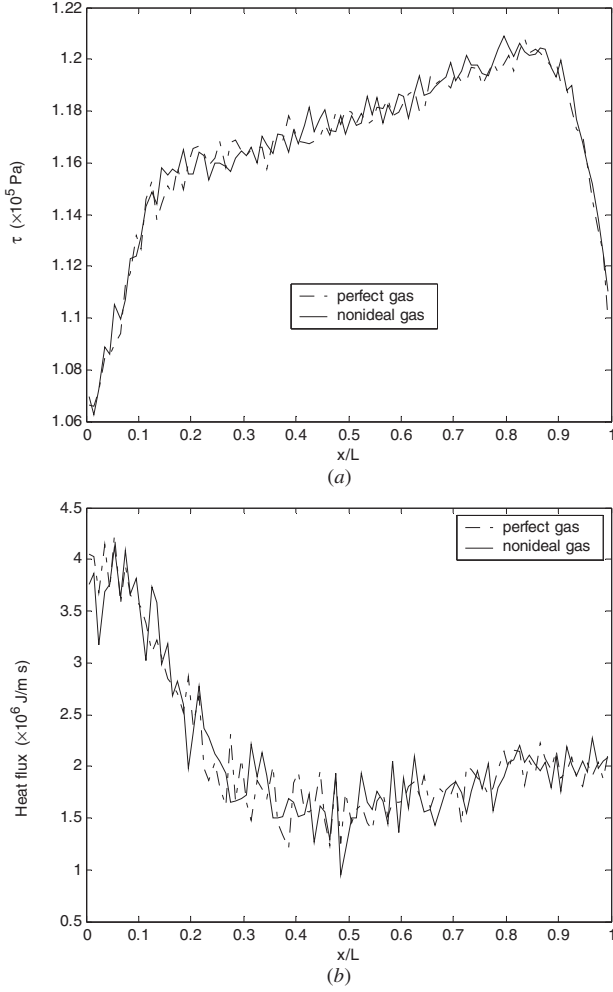


Figure 5. Shear stress and heat flux distributions on the wall surface for a $0.05 \mu\text{m} \times 0.01 \mu\text{m}$ channel at $P_{\text{in}} = 15 \times 10^5$ Pa (case 12). (a) Shear stress distributions; (b) heat flux distributions.

The non-ideal effects on the friction and heat transfer characteristics on the channel wall surface are also investigated. Based on the kinetic theory, the shear stress vector τ is the sum of the tangential momentum fluxes of both the incident and the reflected molecules at each sample step,

$$\tau = \tau_i + \tau_r = \frac{[\sum m\mathbf{u}_i - \sum m\mathbf{u}_r]N_0}{\Delta t(1 \cdot \Delta x)}, \quad (14)$$

where the subscripts 'i' and 'r' are used to denote the incident and reflected molecular streams, respectively; N_0 is the number of gaseous molecules associated with a computational molecule and Δt is the time period of sampling.

The net heat transfer flux q is the sum of the translational and rotational energies of both the incident and the reflected molecules,

$$q = \frac{[(\sum \varepsilon_{\text{tr}} + \sum \varepsilon_{\text{rot}})_i - (\sum \varepsilon_{\text{tr}} + \sum \varepsilon_{\text{rot}})_r]N_0}{\Delta t(1 \cdot \Delta x)}, \quad (15)$$

where ε_{tr} is the molecular translational energy and ε_{rot} is the rotational energy.

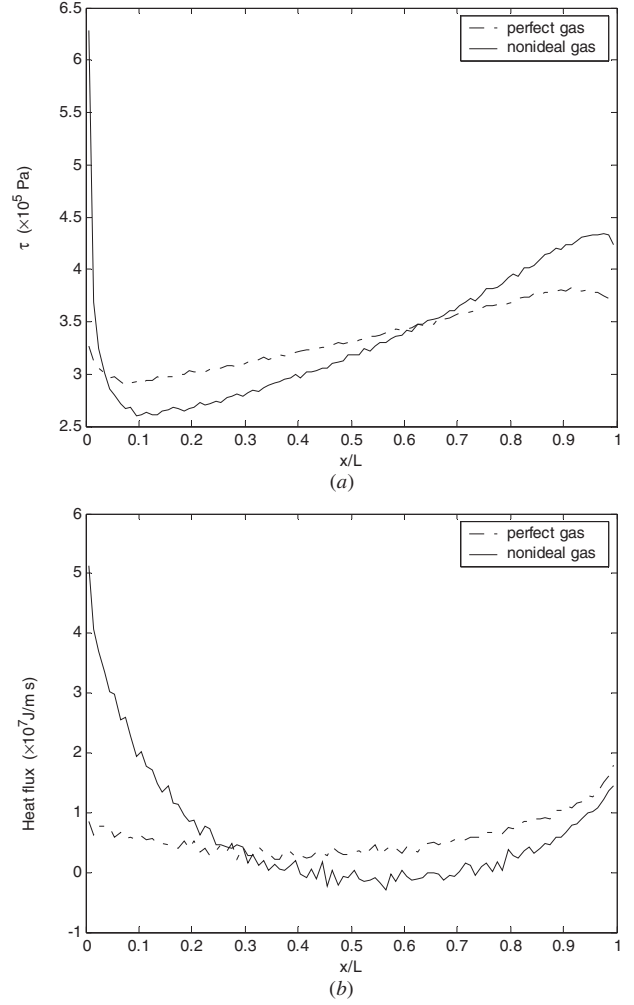


Figure 6. Shear stress and heat flux distributions on the wall surface for a $0.05 \mu\text{m} \times 0.01 \mu\text{m}$ channel at $P_{\text{in}} = 45 \times 10^5$ Pa (case 15). (a) Shear stress distributions; (b) heat flux distributions.

Figure 5 shows the shear stress and heat flux distributions for a $0.05 \mu\text{m} \times 0.01 \mu\text{m}$ channel under a 15×10^5 Pa inlet pressure boundary. The curves have fluctuations due to low gas mean velocities; however, it is clearly shown that the difference between perfect gas and non-ideal gas is very small under such a low driving pressure drop. The shear stress and heat transfer flux results for a 45×10^5 Pa inlet pressure case are shown in figure 6. The differences between perfect gas and non-ideal gas are much larger. This indicates that the van der Waals force greatly affects the channel wall surface friction and heat transfer characteristics for a high-pressure-driven flow case. However, the driving pressure drop is not the only factor that affects the van der Waals effect. Figure 7 shows the results for a $5 \mu\text{m} \times 1 \mu\text{m}$ channel under a 45×10^5 Pa inlet pressure boundary. When the channel size enlarges, the difference between perfect gas and non-ideal gas will decrease.

The result indicates the van der Waals effect on the friction and heat flux of wall surfaces strengthens with the drop in driving pressure and weakens with the channel size increase, for Poiseuille flows.

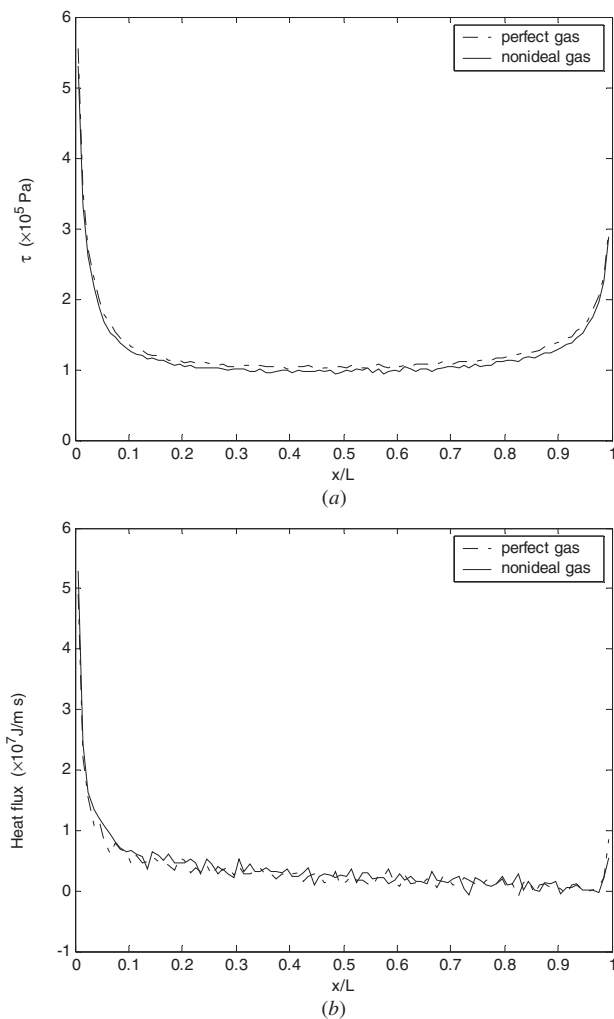


Figure 7. Shear stress and heat flux distributions on the wall surface for a $5 \mu\text{m} \times 1 \mu\text{m}$ channel at $P_{\text{in}} = 45 \times 10^5 \text{ Pa}$ (case 5). (a) Shear stress distributions; (b) heat flux distributions.

3. Conclusions

Non-ideal gas Poiseuille flows in micro- and nanoscale channels were investigated using the direct simulation Monte Carlo method in the consistent Boltzmann algorithm model. Different flow cases were simulated to find the factors affecting the van der Waals effect. The driving pressure drops range from 0.5 to $44 \times 10^5 \text{ Pa}$ and the channel size ranges from microns down to nanometers.

The calculated mass flow rate in a non-ideal gas model is larger than that in a perfect gas model at high inlet pressures. The flow rate differences between perfect gas and non-ideal gas increase with a drop in driving pressure for a given channel. Results for different channel sizes show that for a smaller channel the flow rate differences between both models are bigger. The shear stress and heat flux distributions on the wall surfaces are also compared between perfect gas flow and non-ideal gas flow for different driving pressures and different channel sizes. The results indicate that the van der Waals effect on the friction and on the heat flux to the walls increases as

the driving pressure difference increases, and decreases as the channel size increases.

Acknowledgments

The present work was supported by the National Natural Science Foundation of China (grant no 59995550-2) and National Key Basic Research and Development Programme of China (grant no 1999033106). The authors would like to thank A L Garcia.

References

- [1] Ho C M and Tai Y C 1998 Micro-electro-mechanical-systems (MEMS) and fluid flows *Annu. Rev. Fluid Mech.* **30** 579
- [2] Mohamed G 1999 The fluid mechanics of microdevices-the Freeman scholar lecture *J. Fluids Eng.* **121** 5
- [3] Muntz E P 1989 Rarefied gas dynamics *Annu. Rev. Fluid Mech.* **21** 387
- [4] Ivanov M S and Gimelshein S F 1998 Computational hypersonic rarefied flows *Annu. Rev. Fluid Mech.* **30** 469
- [5] Bird G A 1994 *Molecular Gas Dynamics and the Direct Simulation of Gas Flows* (Clarendon: Oxford)
- [6] Oran E S, Oh C K and Cybyk B Z 1998 Direct simulation Monte Carlo: recent advances and applications *Annu. Rev. Fluid Mech.* **30** 403
- [7] Wagner W 1992 A convergence proof for Bird's direct simulation Monte Carlo method for the Boltzmann equation *J. Stat. Phys.* **66** 1011
- [8] Oh C K, Oran E S and Sinkovits R S 1997 Computations of high-speed, high Knudsen number microchannel flows *J. Thermophys. Heat Transfer* **11** 497
- [9] Liou W W and Fang Y 2001 Heat transfer in microchannel devices using DSMC *J. MEMS.* **10** 274
- [10] Hadjiconstantinou N G and Simek O 2002 Constant-wall-temperature Nusselt number in micro and nano-channels *J. Heat Transfer* **124** 356
- [11] Fan J and Shen C 2001 Statistical simulation of low-speed rarefied gas flows *J. Comput. Phys.* **167** 393
- [12] Sun Q and Boyd I D 2002 A direct simulation method for subsonic, microscale gas flows *J. Comput. Phys.* **179** 400
- [13] Wang M R and Li Z X 2003 Similarity of ideal gas flow at different scales *Sci. China E.* **46** 661
- [14] Hash D B and Hassan H A 1994 Direct simulation of diatomic gas using the generalized hard sphere model *J. Thermophys. Heat Transfer* **8** 758
- [15] Fan J 2002 A generalized soft-sphere model for Monte Carlo simulation *Phys. Fluids* **14** 4399
- [16] Alexander F J, Garcia A L and Alder B J 1995 A consistent Boltzmann algorithm *Phys. Rev. Lett.* **74** 5212
- [17] Montanero J M and Santos A 1996 Monte Carlo simulation method for the Enskog equation *Phys. Rev. E* **54** 438
- [18] Montanero J M and Santos A 1997 Simulation of Enskog equation a la Bird *Phys. Fluids* **9** 2057
- [19] Frezzotti A 1997 Particle scheme for the numerical solution of the Enskog equation *Phys. Fluids* **9** 1329
- [20] Kortemeyer G, Daffin F and Bauer W 1996 Nuclear flow in consistent Boltzmann algorithm models *Phys. Lett. B* **374** 25
- [21] Hadjiconstantinou N G, Garcia A L and Alder B J 2000 The surface properties of a van der Waals fluid *Physica A* **281** 337
- [22] Alexander F J, Garcia A L and Alder B J 1997 The consistent Boltzmann algorithm for the van der Waals equation of state *Physica A* **240** 196

- [23] Garcia A L, Alexander F J and Alder B J 1997 A particle method with adjustable transport properties—the generalized consistent Boltzmann algorithm *J. Stat. Phys.* **89** 403
- [24] Garcia A L and Wagner W 2002 Some new properties of the kinetic equation for the consistent Boltzmann algorithm *Transp. Theory Stat. Phys.* **31** 579
- [25] Schram P P J M 1991 *Kinetic Theory of Gas and Plasmas* (Dordrecht: Kluwer)
- [26] Aston J G and Fritz J J 1959 *Thermodynamics and Statistical Thermodynamics* (New York: Wiley)
- [27] Garcia A L and Wagner W 2000 Time step truncation error in direct simulation Monte Carlo *Phys. Fluids* **12** 2621–33
- [28] Alexander F J, Garcia A L and Alder B J 1998 Cell size dependence of transport coefficients in stochastic particle algorithm *Phys. Fluids* **10** 1540–2
- Alexander F J, Garcia A L and Alder B J 2000 Cell size dependence of transport coefficients in stochastic particle algorithm *Phys. Fluids* **12** 731 (erratum)
- [29] Liou W W and Fang Y 2000 Implicit boundary conditions for direct simulation Monte Carlo method in MEMS flow predictions *Comput. Model. Eng. Sci.* **4** 119